Available on CMS information server

CMS CR -2009/027

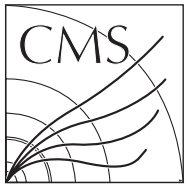

The Compact Muon Solenoid Experiment

Conference Report

Mailing address: CMS CERN, CH-1211 GENEVA 23, Switzerland

09 January 2009 (v3, 26 January 2009)

Forward physics with CMS

Samim Erhan[1], Salim Cerci[2], Monika Grothe[3], Jonathan Hollar[4], Antonio Vilela Pereira[5]

[1]) *University of California, Los Angeles, Los Angeles, California, USA*

[2]) *Cukurova University, Adana, Turkey*

[3]) *University of Wisconsin, Madison, Wisconsin, USA*

[4]) *Lawrence Livermore National Laboratory, Livermore, California, USA*

[5]) *Universitá di Torino e Sezione dell' INFN, Torino, Italy*

on behalf of the CMS collaboration

Abstract

We describe several example analyses of the CMS forward physics program: A feasibility study for observing W production in single diffractive dissociation, the analysis of exclusive $\mu\mu$ production and the measurement of very low-x parton distributions and search for evidence of BFKL dynamics with forward jets.

Presented at *HERA-LHC Workshop,2006 - 2008,Geneve,Switzerland,31/12/2008*

Forward physics with CMS

Samim Erhan[1]*, Salim Cerci*[2]*, Monika Grothe*[3]*, Jonathan Hollar*[4]*, Antonio Vilela Pereira*[5]
on behalf of the CMS collaboration
[1]University of California, Los Angeles, Los Angeles, California, USA
[2]Cukurova University, Adana, Turkey
[3]University of Wisconsin, Madison, Wisconsin, USA
[4]Lawrence Livermore National Laboratory, Livermore, California, USA
[5]Universita di Torino e Sezione dell' INFN, Torino, Italy

Abstract
We describe several example analyses of the CMS forward physics program: A feasibility study for observing W production in single diffractive dissociation, the analysis of exclusive $\mu\mu$ production and the measurement of very low-x parton distributions and search for evidence of BFKL dynamics with forward jets.

1 Introduction

The CMS Experiment has a rich and broad forward physics program with measurements that can be realized from the start of the LHC [1–6]. The CMS detectors in the forward region allow an experimental program to be carried out that reaches beyond the traditional forward gap physics, such as soft and hard single diffraction and double Pomeron exchange physics, and also includes the study of $\gamma\gamma$ and γp interactions, energy and particle flow measurements relevant for understanding multi-parton interactions for tuning of Monte Carlo event generators, jet-gap-jet events to understand the origin of these event topologies, and forward jets and forward Drell-Yan processes at 14 TeV center-of-mass energies. Topics of soft and hard diffraction include but are not limited to:

1. Dependence of the diffractive cross sections on ξ, t and $\mathrm{M_x}$ as fundamental quantities of non-perturbative QCD.
2. Gap survival dynamics and multi-gap event topologies.
3. Production of jets, $W, \mathrm{J}/\psi, \mathrm{b}$ and t quarks, hard photons in hard diffraction.
4. Double Pomeron Exchange events as gluon factory.
5. Central exclusive Higgs boson production.
6. SUSY and other low mass exotics in exclusive processes.
7. Proton light cone studies.

CMS shares its interaction point (IP) with the TOTEM experiment [7]. The two experiments plan [8] to join their resources and use common trigger and data acquisition systems to increase their forward physics potential.

The studies presented in the following assume no event pile-up, i.e. are analyses to be carried out during the low pile-up, start-up phase of the LHC. In addition, CMS is studying a proposal to install tracking and time-of-flight detectors at 420 m from the IP [9], which has the potential of adding discovery physics, notably central exclusive Higgs production, to the forward physics program of CMS.

For space limitations, in this paper, we describe only three processes as examples of the CMS forward physics program. After a brief description of the forward detector instrumentation around the CMS IP, section III covers a feasibility study on observing W production in single diffractive dissociation. The analysis of exclusive $\mu\mu$ production is discussed in Section IV and the possibility of measuring very low-x parton distributions and of looking for evidence of BFKL signatures with forward jets is described in Section V.

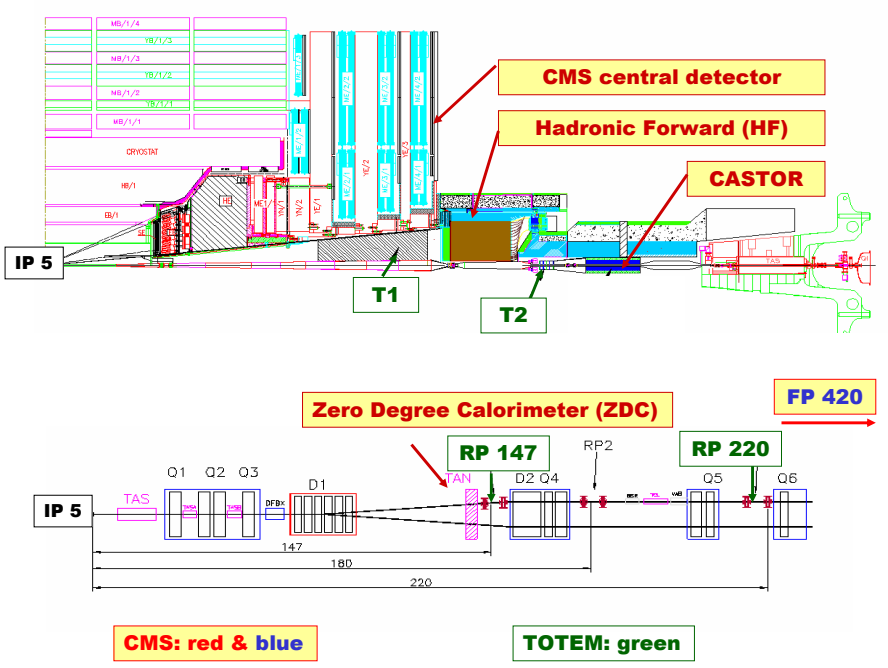

Fig. 1: Layout of the forward detectors around the CMS interaction point.

2 Forward detectors around the CMS interaction point

Forward physics at the LHC covers a wide range of diverse physics subjects that have in common that particles produced at small polar angles, θ, and hence large values of rapidity provide a defining characteristic. At the Large-Hadron-Collider (LHC), where proton-proton collisions occur at center-of-mass energies of 14 TeV, the maximal possible rapidity is $y_{max} = \ln \frac{\sqrt{s}}{m_\pi} \sim 11.5$. The central components of CMS are optimized for efficient detection of processes with large polar angles and hence high transverse momentum, p_T. They extend down to about $|\theta| = 1^\circ$ from the beam axis or $|\eta| = 5$, where $\eta = -\ln[\tan(\theta/2)]$ is the pseudorapidity. In the forward region, the central CMS components are complemented by several CMS [10] and TOTEM subdetectors with coverage beyond $|\eta| = 5$, see figure 1. TOTEM is an approved experiment at the LHC for precision measurements of the pp elastic and total cross sections. The combined CMS and TOTEM apparatus comprises two suites of calorimeters with tracking detectors in front plus near-beam proton taggers. The CMS Hadron Forward (HF) calorimeter with the TOTEM telescope T1 in front covers the region $3 < |\eta| < 5$, the CMS CASTOR calorimeter with the TOTEM telescope T2 in front covers $5.2 < |\eta| < 6.6$. The CMS ZDC calorimeters are installed at the end of the straight LHC beam-line section, at a distance of ± 140 m from the IP. Near-beam proton taggers will be installed by TOTEM at ± 147 m and ± 220 m from the IP. The kinematic coverage of the combined CMS and TOTEM apparatus is unprecedented at a hadron collider. The CMS and TOTEM collaborations have described the considerable physics potential of joint data taking in a report to the LHCC [8]. Further near-beam proton taggers in combination with very fast timing detectors to be installed at ± 420 m from the IP (FP420) are in the proposal stage in CMS. FP420 would give access to possible discovery processes in forward physics at the LHC [9].

2.1 The CMS forward calorimeters HF, CASTOR, ZDC

The forward part of the hadron calorimeter, HF, is located 11.2 m from the interaction point. It consists of steel absorbers and embedded radiation hard quartz fibers, which provide a fast collection of Cherenkov

light. Each HF module is constructed of 18 wedges in a nonprojective geometry with the quartz fibers running parallel to the beam axis along the length of the iron absorbers. Long (1.65 m) and short (1.43 m) quartz fibers are placed alternately with a separation of 5 mm. These fibers are bundled at the back of the detector and are read out separately with phototubes.

The CASTOR calorimeters are octagonal cylinders located at ~ 14 m from the IP. They are sampling calorimeters with tungsten plates as absorbers and fused silica quartz plates as active medium. The plates are inclined by 45° with respect to the beam axis. Particles passing through the quartz emit Cherenkov photons which are transmitted to photomultiplier tubes through aircore lightguides. The electromagnetic section is 22 radiation lengths X_0 deep with 2 tungsten-quartz sandwiches, the hadronic section consists of 12 tungsten-quartz sandwiches. The total depth is 10.3 interaction lengths λ_l. The calorimeters are read out segmented azimuthally in 16 segments and logitudinally in 14 segments. They do not have any segmentation in η. The CASTOR coverage of $5.2 < |\eta| < 6.6$ closes hermetically the CMS calorimetric pseudorapidity range over 13 units. Currently, funding is available only for a CASTOR calorimeter on one side of the IP. Installation is foreseen for 2009.

The CMS Zero Degree Calorimeters, ZDC, are located inside the TAN absorbers at the ends of the straight section of the LHC beamline, between the LHC beampipes, at ± 140 m distance on each side of the IP. They are very radiation-hard sampling calorimeters with tungsten plates as absorbers and as active medium quartz fibers read out via aircore light guides and photomultiplier tubes. The electromagnetic part, $19X_0$ deep, is segmented into 5 units horizontally, the hadronic part into 4 units in depth. The total depth is 6.5 λ_l. The ZDC calorimeters have 100% acceptance for neutral particles with $|\eta| > 8.4$ and can measure 50 GeV photons with an energy resolution of about 10%. The ZDC calorimeters are already installed and will be operational in 2009.

2.2 The TOTEM T1 and T2 telescopes

The TOTEM T1 telescope consists of two arms symmetrically installed around the CMS IP in the endcaps of the CMS magnet, right in front of the CMS HF calorimeters and with η coverage similar to HF. Each arm consists of 5 planes of Cathod Strip Chambers (CSC) which measure 3 projections per plane, resulting in a spatial resolution of 0.36 mm in the radial and 0.62 mm in the azimuthal coordinate in test beam measurements. The two arms of the TOTEM T2 telescope are mounted right in front of the CASTOR calorimeters, with similar η coverage. Each arm consists of 10 planes of 20 semi-circular modules of Gas Electron Multipliers (GEMs). The detector read-out is organized in strips and pads, a resolution of 115 μm for the radial coordinate and of 16 μrad in azimuthal angle were reached in prototype test beam measurements. A more detailed description can be found in [11].

2.3 Near-beam proton taggers

The LHC beamline with its magnets is essentially a spectrometer in which protons slightly off the beam momentum are bent sufficiently to be detectable by means of detectors inserted into the beam-pipe. At high luminosity at the LHC, proton tagging is the only means of detecting diffractive and γ mediated processes because areas of low or no hadronic activity in the detector are filled in by particles from overlaid pile-up events.

The TOTEM proton taggers at ± 220 m at nominal LHC optics have acceptance for scattered protons from the IP for $0.02 < \xi < 0.2$. Smaller values of ξ, $0.002 < \xi < 0.02$, can be achieved with proton taggers at ± 420 m. The FP420 proposal [9] foresees employing 3-D Silicon, an extremely radiation hard novel Silicon technology, for the proton taggers, and additional fast timing Cherenkov detectors for the rejection of protons from pile-up events. The proposal is currently under consideration in CMS. If approved, installation could proceed in 2010, after the LHC start-up.

Forward proton tagging capabilities enhance the physics potential of CMS. They would render possible a precise measurement of the mass and quantum numbers of the Higgs boson should it be

discovered by traditional searches. They also augment the CMS discovery reach for Higgs production in the minimal supersymmetric extension (MSSM) of the Standard Model (SM) and for physics beyond the SM in γp and $\gamma\gamma$ interactions. The proposed FP420 detectors and their physics potential are discussed in [12].

3 Observation of single-diffractive W production with CMS: a feasibility study

The single-diffractive (SD) reaction $pp \to Xp$, where X includes a W boson (Fig. 2) is studied to demonstrate the feasibility of observing SD W production at CMS given an integrated effective luminosity for single interactions of 100 pb^{-1}. Only $W \to \mu\nu$ decay mode is considered in this analysis [2].

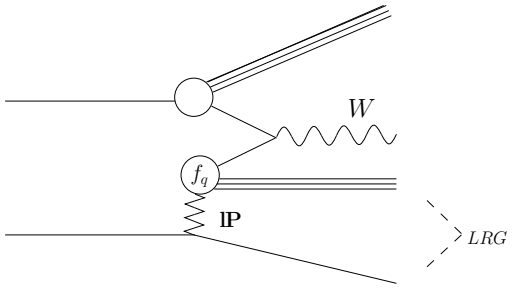

Fig. 2: Sketch of the single-diffractive reaction $pp \to Xp$ in which X includes a W boson. The symbol $I\!P$ indicates the exchange with the vacuum quantum numbers (Pomeron). The large rapidity gap (LRG) is also shown.

The analysis relies on the extended forward coverage of the CMS forward calorimeters, that cover the pseudo-rapidity range of $3 < |\eta| < 5$. Additional coverage at $-6.6 < \eta < -5.2$ is assumed by means of the CASTOR calorimeter.

Single diffractive W production was simulated by using the POMWIG generator [13], version v2.0 beta. For the diffractive PDFs and the Pomeron flux, the result of the NLO H1 2006 fit B [14] was used. A rapidity gap survival probability of 0.05, as predicted in Ref. [15], is assumed. For non-diffractive W production, the PYTHIA generator [16] was used. With the assumed numbers for the cross sections, the ratio of diffractive to inclusive yields is around 0.3%.

3.1 Event Selection and Observation of SD W Production

3.1.1 $W \to \mu\nu$ selection

The selection of the events with a candidate W decaying to $\mu\nu$ is the same as that used in Ref. [17]. Events with a candidate muon in the pseudo-rapidity range $|\eta| > 2.0$ and transverse momentum $p_T < 25$ GeV were rejected, as were events with at least two muons with $p_T > 20$ GeV. Muon isolation was imposed by requiring $\sum p_T < 3$ GeV in a cone with $\Delta R < 0.3$. The transverse mass was required to be $M_T > 50$ GeV. The contribution from top events containing muons was reduced by rejecting events with more than 3 jets with $E_T > 40$ GeV (selected with a cone algorithm with radius of 0.5) and requiring that the acoplanarity ($\zeta = \pi - \Delta\phi$) between the muon and the direction associated to $E_T^{\rm miss}$ be less than 1 rad. Approximately 2,400 SD W events and 600,000 non-diffractive W events per 100 pb^{-1} are expected to pass these cuts.

3.1.2 Diffractive selection and Evidence for SD W Production

Diffractive events have, on average, lower multiplicity both in the central region (lower underlying event activity) and in the hemisphere that contains the scattered proton, the so-called "gap side", than non-diffractive events.

The gap side was selected as that with lower energy sum in the HF. A cut was then placed on the multiplicity of tracks with $p_T > 900$ MeV and $|\eta| < 2$. For the events passing this cut, multiplicity distributions in the HF and CASTOR calorimeters in the gap side were studied, from which a diffractive sample can be extracted.

Figure 3 shows the HF tower multiplicity vs the CASTOR ϕ sector multiplicity for events with central track multiplicity $N_{\rm track} \leq 5$. Since CASTOR will be installed at first on the negative side of the interaction point, only events with the gap on that side (as determined with the procedure discussed above) were considered. The CMS software chain available for this study did not include simulation/reconstruction code for CASTOR; therefore, the multiplicity of generated hadrons with energy above a 10 GeV threshold in each of the CASTOR azimuthal sectors was used.

The top left and top right plots show the distributions expected for the diffractive W events with generated gap in the positive and negative Z direction, respectively. The few events in the top left plot are those for which the gap-side determination was incorrect. The non-diffractive W events have on average higher multiplicities, as shown in the bottom left plot. Finally, the bottom right plot shows the sum of the POMWIG and PYTHIA distributions – this is the type of distribution expected from the data.

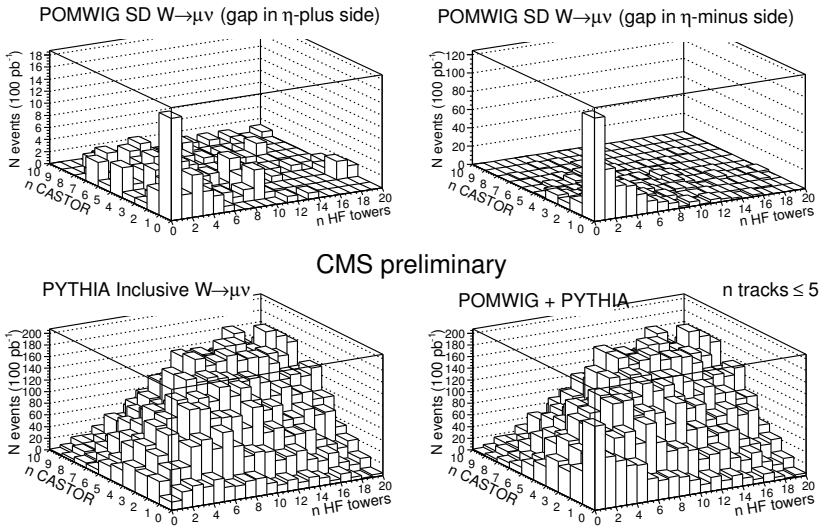

Fig. 3: HF tower multiplicity vs CASTOR sector multiplicity distribution for events with track multiplicity in the central tracker $N_{\rm track} \leq 5$.

A simple way to isolate a sample of diffractive events from these plots is to use the zero-multiplicity bins, where the diffractive events cluster and the non-diffractive background is small.

The HF plus CASTOR combination yields the best signal to background ratio. When an integrated effective luminosity for single interactions of 100 pb^{-1} becomes available, SD $W \to \mu\nu$ production can then be observed with $\mathcal{O}(100)$ signal events. The situation is even more favorable for SD dijet production where a recently completed study [3] arrives at $\mathcal{O}(300)$ SD dijet events per 10 pb^{-1} of integrated effective luminosity for single interactions. With an observation of a number of signal events of this size, it should be possible to exclude values of rapidity gap survival probability at the lower end of the spectrum of theoretical predictions. A method to establish that the observed population of the zero-multiplicity bins is indeed indicative of the presence of SD events in the data is described in [3]. The method is based on the observation that the size of the SD signal in the zero-multiplicity bins can be controlled in a predictable way when the cuts for enhancing the SD signal are modified.

The main background other than non-diffractive W production consists of SD W production with proton-dissociation, $pp \to XN$, where X contains a W boson and N is a low-mass state into which

the proton has diffractively dissociated. A study of proton-dissociation has been carried out in Ref. [4], where it has been shown that about 50% of the proton-dissociative background can be rejected by vetoing events with activity in the CMS Zero Degree Calorimeter (ZDC), which provides coverage for neutral particles for $|\eta| > 8.1$. The net effect is to enhance the diffractive signal in the zero multiplicity bin of Fig. 3 by about 30%.

4 Exclusive $\gamma\gamma \to \ell^+\ell^-$ and $\gamma p \to \Upsilon p \to \ell^+\ell^- p$

Exclusive dilepton production in pp collisions at CMS can occur through the processes $\gamma\gamma \to \ell^+\ell^-$ and $\gamma p \to \Upsilon p \to \ell^+\ell^- p$. The first is a QED process, making it an ideal sample for luminosity calibration at the LHC. The second will allow studies of vector meson photoproduction at energies significantly higher than previous experiments. Zero pileup is assumed for this study [4]. Both signal processes are characterized by the presence of two same-flavor opposite-sign leptons back-to-back in $\Delta\phi$, and with equal $|p_T|$. In the no-pileup startup scenario assumed here, the signal is also distinguished by having no calorimeter activity that is not associated with the leptons, and no charged tracks in addition to the two signal leptons. This exclusivity requirement is implemented by requiring that there be no more than 5 "extra" calorimeter towers with $E > 5$ GeV, where extra towers are defined as those separated from either of the lepton candidates by $\Delta R > 0.3$ in the $\eta - \phi$ plane. The track multiplicity is required to be < 3. The dominant inelastic photon-exchange background is reduced by requiring no activity in the CASTOR calorimeter (covering $5.2 < \eta < 6.6$) or the Zero Degree Calorimeter (covering $|\eta| > 8.2$). The residual background from non-photon exchange processes is estimated from an exponential fit to the sideband of the extra calorimeter towers distribution, resulting in a background estimate of approximately 39 events in 100 pb^{-1}, which is small compared to the inelastic background.

The expected $\gamma\gamma \to \mu^+\mu^-$ signal yields in 100 pb^{-1} are $N_{elastic}(\gamma\gamma \to \mu^+\mu^-) = 709 \pm 27$, and $N_{inelastic}(\gamma\gamma \to \mu^+\mu^-) = 223 \pm 15 \pm 42(model)$. Without the ZDC and Castor vetoes, the singly inelastic contribution would be significantly larger: $N_{inelastic}(\gamma\gamma \to \mu^+\mu^-) = 636 \pm 25 \pm 121(model)$. In the $\gamma\gamma \to e^+e^-$ channel, the expected yields are significantly smaller. After all trigger and selection criteria are applied the expected elastic signal yields in 100 pb^{-1} are: $N_{elastic}(\gamma\gamma \to e^+e^-) = 67 \pm 8$, and $N_{inelastic}(\gamma\gamma \to e^+e^-) = 31 \pm 6 \pm 6(model)$. Without the ZDC and Castor vetoes, the singly inelastic contribution would be: $N_{inelastic}(\gamma\gamma \to e^+e^-) = 82 \pm 9 \pm 15(model)$. The elastic $\gamma\gamma \to \mu^+\mu^-$ signal can be separated from the inelastic background for luminosity measurements using the $\Delta\phi$ and Δp_T distributions (Figure 4), while the Υ photoproduction signal can be further distinguished by performing a fit to the dimuon invariant mass distribution (Figure 5).

We conclude that with $100 pb^{-1}$ of integrated luminosity, a large sample of $\gamma\gamma \to \mu^+\mu^-$ and $\gamma p \to$

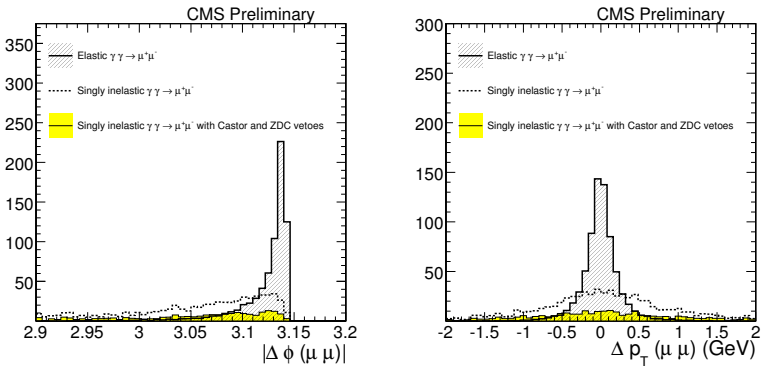

Fig. 4: Distributions of $|\Delta\phi(\mu^+\mu^-)|$ (left) and $|\Delta p_T(\mu^+\mu^-)|$ (right) for $\gamma\gamma \to \mu^+\mu^-$ events passing all selection requirements. The elastic signal is denoted by the open histogram, the inelastic background is shown with no CASTOR/ZDC vetos (dashed line), and with the veots described in the text (solid histogram).

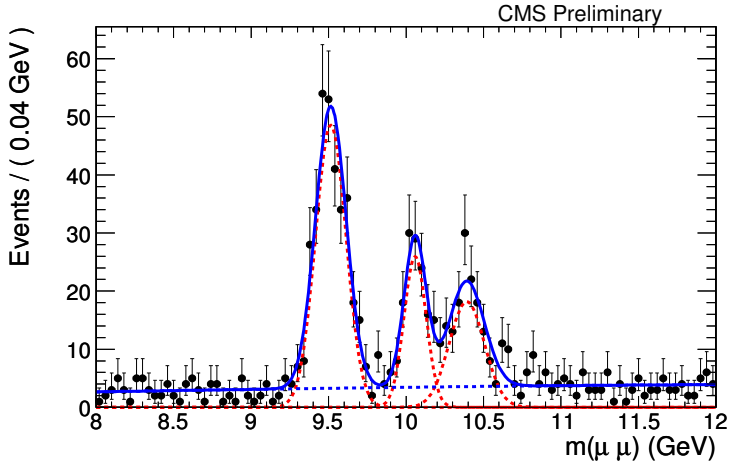

Fig. 5: Dimuon invariant mass in the range $8 < m(\mu^+\mu^-) < 12$ GeV. The lines show the result of a fit, where the dashed line is the Υ component, the dotted line is the two-photon continuum, and the solid line is the sum of the two.

$\Upsilon p \to \mu^+\mu^- p$ events can be triggered and reconstructed in the CMS detector, using a common selection for both samples. With minimal pileup these events can be cleanly distinguished from the dominant backgrounds. The Υ sample will allow measurements of cross-sections and production dynamics at significantly higher energies than previous experiments, while the $\gamma\gamma \to \ell^+\ell^-$ sample will serve as a calibration sample for luminosity studies.

5 Forward jets reconstruction in HF

5.1 Introduction

The parton distribution functions (PDFs) in the proton have been studied in detail in deep-inelastic-scattering (DIS) ep collisions at HERA [18]. For decreasing parton momentum fraction $x = p_{parton}/p_{hadron}$, the gluon density is observed to grow rapidly as $xg(x, Q^2) \propto x^{-\lambda(Q^2)}$, with $\lambda \approx 0.1$–0.3 rising logarithmically with Q^2. As long as the densities are not too high, this growth is described by the Dokshitzer-Gribov-Lipatov-Altarelli-Parisi (DGLAP) [19] or by the Balitski-Fadin-Kuraev-Lipatov (BFKL) [20] evolution equations which govern, respectively, parton radiation in Q^2 and x. Experimentally, direct information on the parton structure and evolution can be obtained in hadron-hadron collisions from the perturbative production of e.g. jets or prompt γ's, which are directly coupled to the parton-parton scattering vertex. The measurement of jets with transverse momentum $p_T \approx 20$ GeV in the CMS forward calorimeters (HF, $3< |\eta| <5$ and CASTOR, $5.1< |\eta| <6.6$) will allow one to probe x values as low as $x_2 \approx 10^{-5}$. Figure 6 (right) shows the actual $\log(x_{1,2})$ distribution for two-parton scattering in p-p collisions at 14 TeV producing at least one jet above 20 GeV in the HF and CASTOR acceptances. Full detector simulation and reconstruction packages were used in obtaining these results.

5.2 Forward jets reconstruction in HF

Jets in CMS are reconstructed at the generator- and calorimeter-level using 3 different jet algorithms [5]: iterative cone [10] with radius of $\mathcal{R} = 0.5$ in (η, ϕ), SISCone [22] ($\mathcal{R} = 0.5$), and the Fast-k_T [23] (E_{seed} = 3 GeV and E_{thres} = 20 GeV). The p_T resolutions for the three different algorithms are very similar: $\sim$18% at p_T $\sim$20 GeV decreasing to $\sim$12% for $p_T \gtrsim$100 GeV (Fig. 6, Left). The position (η, ϕ) resolutions (not shown here) for jets in HF are also very good: $\sigma_{\phi,\eta}$ = 0.045 at p_T = 20 GeV, improving to $\sigma_{\phi,\eta} \sim 0.02$ above 100 GeV.

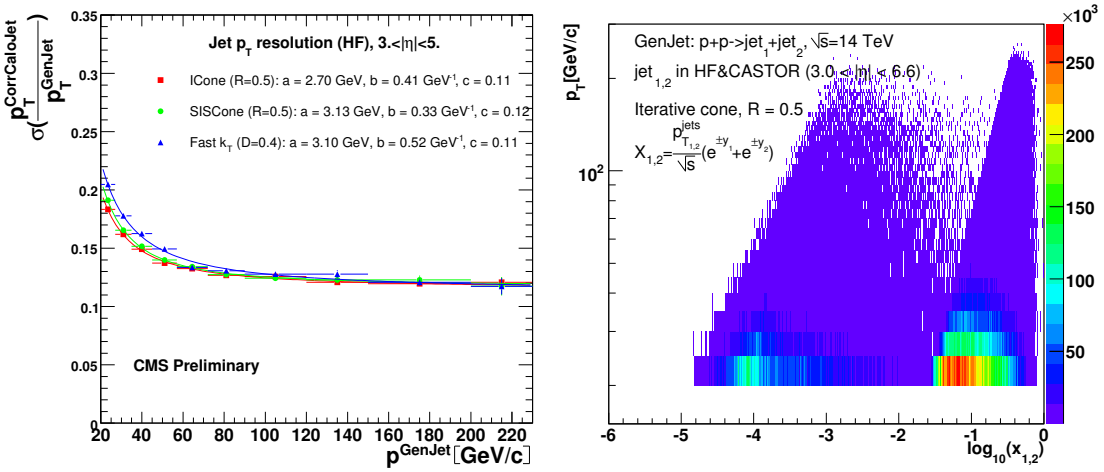

Fig. 6: Energy resolution as a function of p_T for the ICone, SISCone (with cone sizes $R = 0.5$) and FastKt ($D = 0.4$) algorithms for jets reconstructed in HF ($3. < |\eta| < 5.$). The resolutions are fitted to $f(p_T) = \sqrt{\left(\frac{a}{p_T^{gen}}\right)^2 + \left(\frac{b}{\sqrt{p_T^{gen}}}\right)^2 + c^2}$ with the parameters quoted in the legend (Left). Log($x_{1,2}$) distribution of two partons producing at least one jet above p_T = 20 GeV within HF ($3 < |\eta| < 5$) and CASTOR ($5.1 < |\eta| < 6.6$) in p-p collisions at $\sqrt{s}$ = 14 TeV (Right).

5.3 Single inclusive jet p_T spectrum in HF

In this section, we present the reconstructed forward jet yields as a function of p_T for 1 pb^{-1} integrated luminosity. Figure 7 (left) shows reconstructed (and corrected for energy resolution smearing) single inclusive forward jet spectrum in HF in p-p collisions at 14 TeV for a total integrated luminosity of 1 pb^{-1} compared to fastNLO jet predictions [24] using various PDFs (MRST03 and CTEQ6.1M). Figure 7 (right) shows percent differences between the reconstructed forward jet p_T spectrum and two fastNLO predictions (CTEQ6.1M and MRST03 PDFs). The error bars include the statistical and the energy-resolution smearing errors. The solid curves indicate the propagated uncertainty due to the jet-energy scale (JES) error for "intermediate" (10% decreasing to a constant 5% for $p_T > 50$ GeV/c) conditions. If the JES can be improved below 10% (such as in the "intermediate" scenario considered), our measurement will be more sensitive to the underlying PDF. The main conclusion of this part of the study is that the use of the forward jet measurement in HF to constrain the proton PDFs in the low-x range will require careful studies of the HF jet calibration.

References

[1] CERN-LHCC-2006-021 (2006).

[2] CMS Collaboration, CMS PAS DIF-07-002 (2007).

[3] CMS Collaboration, CMS PAS FWD-08-002 (2008).

[4] CMS Collaboration, CMS PAS DIF-07-001 (2007).

[5] CMS Collaboration, CMS PAS FWD-08-001 (2008).

[6] M. Grothe, in proceedings of the workshop on high-energy photon collisions at the LHC, D. D'Enterria *et al.* (eds), CERN, Geneva, Switzerland, 2008.

[7] TOTEM Collaboration: Letter of Intent, CERN-LHCC 97-49; Technical Proposal, CERN-LHCC 99-7; Technical Design Report, CERN-LHCC-2004-002.

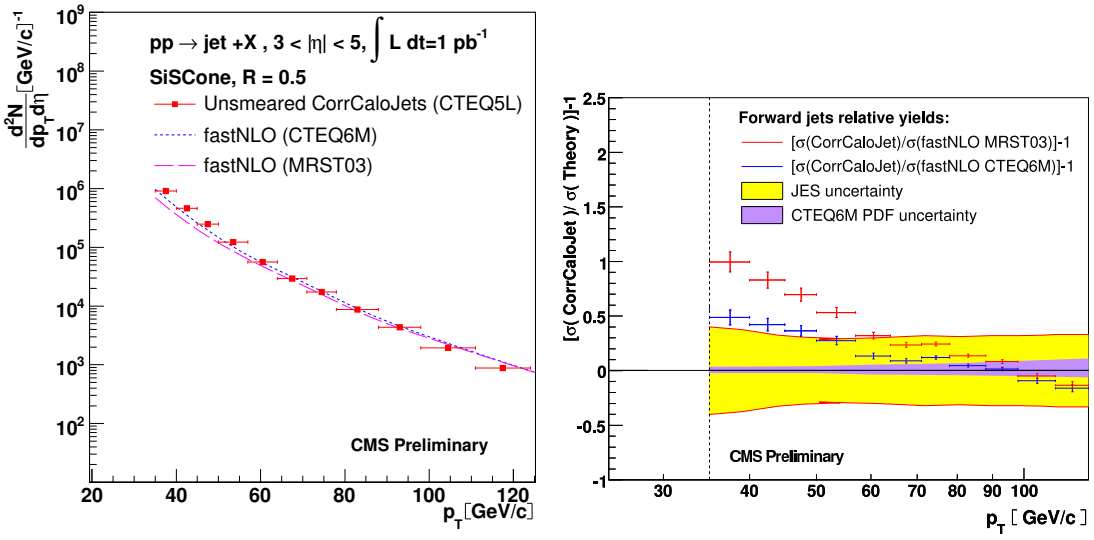

Fig. 7: Left: The forward jet yields for a total integrated luminosity of 1 pb^{-1}. Right: Percent differences between the reconstructed forward jet p_T spectrum and two fastNLO predictions (CTEQ6.1M and MRST03 PDFs). The solid curves indicate the propagated uncertainty due to the jet-energy scale (JES) error for "intermediate" 10% decreasing to a constant 5% for $p_T > 50$ GeV/c conditions.

[8] M. Albrow *et al.* [CMS and TOTEM Collaborations], CERN/LHCC 2006-039/G-124.

[9] FP420 Collaboration, arXiv:0806.0302, [hep-ex].

[10] CMS Collaboration, CERN-LHCC-2006-001 (2006).

[11] TOTEM Collaboration, these proceedings.

[12] P. Bussey, these proceedings.

[13] B. E. Cox and J. R. Forshaw, Comput. Phys. Commun. **144** (2002) 104.

[14] A. Aktas *et al.*, [H1 Collaboration], Eur. Phys. J. C **48** (2006) 715.

[15] V. A. Khoze, A. D. Martin and M. G. Ryskin, Phys. Lett. B **643** (2006) 93.

[16] T. Sjostrand, S. Mrenna and P. Skands, JHEP **0605** (2006) 026.

[17] CMS Collaboration, CMS PAS EWK-07-002 (2007).

[18] M. Klein and R. Yoshida, arXiv:0805.3334 [hep-ex].

[19] V.N. Gribov and L.N. Lipatov, Sov. Journ. Nucl. Phys. **15** (1972) 438; G. Altarelli and G. Parisi, Nucl. Phys. **B126** (1977) 298; Yu. L. Dokshitzer, Sov. Phys. JETP **46** (1977) 641.

[20] L.N. Lipatov, Sov. J. Nucl. Phys. **23** (1976) 338; E.A. Kuraev, L.N. Lipatov and V.S. Fadin, Zh. Eksp. Teor. Fiz **72**, (1977) 3; I.I. Balitsky, L.N. Lipatov, Sov. J. Nucl. Phys. **28** (1978) 822.

[21] CMS Physics TDR, Volume 1, CERN-LHCC-2006-001, 2 February 2006

[22] G. P. Salam and G.Soyez, JHEP05 (2007) 086

[23] M.Cacciari and G. P. Salam, Phys. Lett. B **641** (2006) 57.

[24] T. Kluge, K. Rabbertz, M. Wobisch, arXiv:hep-ph/0609285; K. Rabbertz, private communication.